Hindawi
Geofluids
Volume 2022, Article ID 4145219, 18 pages
https://doi.org/10.1155/2022/4145219

Research Article

Prediction of the Control Effect of Fractured Leakage in Unconventional Reservoirs Using Machine Learning Method

Lei Pu,[1,2,3] **Jianjian Song**,[1,2,3] **Mingbiao Xu**,[1,2] **Jun Zhou**,[4] **Peng Xu**,[1,2,3] **and Shanshan Zhou**[1,2,3]

[1]*School of Petroleum Engineering, Yangtze University, Wuhan 430100, China*
[2]*Cooperative Innovation Center of Unconventional Oil and Gas, Yangtze University (Ministry of Education & Hubei Province), Wuhan, Hubei 430100, China*
[3]*Key Laboratory of Drilling and Production Engineering for Oil and Gas, Hubei Province, Wuhan Hubei, China 430100*
[4]*PetroChina Xinjiang Oilfield Development Company, Karamay, Xinjiang, China 834000*

Correspondence should be addressed to Jianjian Song; songjian629@yangtzeu.edu.cn
and Mingbiao Xu; xumingbiao@yangtzeu.edu.cn

Received 1 April 2022; Revised 25 May 2022; Accepted 3 June 2022; Published 24 June 2022

Academic Editor: Dong Feng

Bridging plugging is the most used method of plugging in unconventional oil reservoirs, and many factors affect the effect of bridging and plugging. Since the laboratory cannot simulate the actual leakage size of the lost formation and the corresponding leakage plugging process at the drilling site, the laboratory experiment results cannot reflect the actual leakage plugging construction effect. Aiming at the problem of frequent fracture leakage during drilling in Chepaizi block, Xinjiang, China, this paper proposes a set of machine learning methods based on a neural network. Three types of factors and 14 parameters with a strong correlation with the leakage control effect were screened out. Three categories of factors include construction parameters, choice of plugging material, and fluid properties of the carrier fluid. The training was carried out based on the collected field data, the appropriate activation function was set, and the deep well network structure was optimized. By improving the field plugging measures in the later period, the model was verified by these actual cases, and the results showed that the established model produced the highest R^2 of 0.974, has a good fit, and predicts well.

1. Introduction

In unconventional reservoir formations, leakage is one of the typical complex problems in the drilling process [1]. Faced with the problem of downhole leakage, improper treatment measures will lead to a low success rate of plugging, continuous leakage of drilling fluid, and an increase of lost working hours on-site and even further lead to wellbore scrapping (well abandonment) [2–3]. Carboniferous fractures are developed in the target layer of the Chepaizi block in Xinjiang, China, and loss of return and leakage frequently occurs during the drilling fluid process. Leakage control is a problem that has always plagued the site. Because the field engineer cannot understand the details of the underground lost formation, there is a problem of blindly plugging the leakage, which leads to the current situation of difficult one-time plugging. Frequent leakage problems cost a lot of construction time, and plugging construction takes 15% of the drilling cycle, which significantly increases the drilling cost and cannot meet the strategic needs of low-cost development [4–5].

The bridging plugging method is the most used in the construction of the Chepaizi block due to its simple construction process, low cost, and remarkable effect. Bridging and plugging materials are the key means to restore and enhance wellbore stress. The loss-stopping material establishes a dense, high-strength loss-stopping layer to balance the wellbore liquid column pressure, thereby preventing the propagation of fractures. Corrective borehole strengthening is a method to effectively improve the fracture

resistance of the rock formation by improving the formation closure stress and increasing the hoop stress in the near-wellbore area [6]. In this process, the quality of the plugging layer is related to various factors. Pump speed, pump pressure, the formula of bridging and plugging materials, and the viscosity of drilling fluid or particular plugging slurry will all affect the quality of the plugging layer. Poor quality plugging layer is the main reason for the failure of plugging [7–10].

Due to the significant difference between the actual situation of the leakage layer under the formation and the leakage channel simulated in the laboratory, there are certain limitations to the indoor fracture sealing experiment, and it is impossible to simulate the natural fractures in the formation, as well as the pumping displacement, and the pressure is also beyond the reach of laboratory equipment [11]. Laboratory experiments are lacking through the process of pumping the lost circulation slurry from the wellbore to the fracture. Therefore, according to laboratory experiments, it is often possible to obtain better effective plugging formulas, but the plugging process in the actual field still cannot play a good role. Since the laboratory experiment on the formulation of the plugging slurry is different from field plugging, the indoor plugging experiment method clearly understands the leakage channel [12–14]. However, the site's understanding of the underground leakage formation is vague. However, the loss dynamics, imaging logging data, and other methods have been adopted to infer the size of the leakage channel in the downhole lost formation. However, the cognition of downhole lost formation is limited within a specific range [15–18]. Therefore, it is not easy to choose a plugging method suitable for the site.

Machine learning methods are widely used in the exploration and development of the oil field. The large amount of data generated during the drilling process can solve practical problems in the field through machine learning. Pang et al. [19] extracted 22 comprehensive logging parameters from the drilling process and based on a set of deep learning mixed density network models, and they could reasonably predict the leakage problem. Gul and van Oort [20] avoided the pitfalls of manual measurement by establishing machine learning and deep learning to predict the filtration performance of water-based drilling fluids through fluid properties such as drilling fluid rheology, density, and temperature. Diaz et al. [21] used an artificial neural network to predict the permeability for nine drilling parameters obtained during drilling. Mahmoud et al. [22] compared three machine learning models, trained on 3,162 data sets of 6 (drilling parameters) and real-time prediction of formation lithology. Zhu Z et al. [23] predicted the settlement behavior of rod proppant in fractures through the artificial neural network, and the data set was from 588 practical laboratory experiments. Aiming at the advantages of machine learning methods in data processing, it can improve more accurate guidance for learning more data [24–26]. Machine learning methods seem to be able to replace the methods recommended by the experience of field engineers. These computationally intelligent methods can learn from the experience of plugging projects in this area and give more reasonable recommended methods [27].

According to the artificial neural network to estimate the most reasonable plugging formula, this study aims to evaluate the potential of using artificial neural networks to mine and analyze data from lost circulation plugging construction in the Chepaizi block, Xinjiang, China, and then build an intelligent model to predict lost circulation problems while drilling for the Carboniferous strata in the block. On-site technicians can use the construction effect of leakage to make quick and effective decisions in the face of leakage accidents.

2. The Theoretical Background of Fracture Plugging

2.1. The Missing Geological Conditions of the Chepaizi Block. The Chepaizi block is located on the northwestern margin of the Junggar Basin in Xinjiang, China. During the drilling process of the Chepaizi block, there were frequent leakages, mainly loss-of-return leakage; the loss time of front leakage was mainly distributed between 30 and 120 hours, and the potential leakage risk is high; the success rate of a single leakage plugging is low, and there are many cases of repeated leakage. The leakage situation in the Chepaizi block generally exists in the Carboniferous strata. The Carboniferous volcanic rock reservoirs in the Chepaizi area have developed fractures and have low pressure-bearing capacity. The Carboniferous volcanic rocks in the Chepaizi area have developed fractures, mainly oblique fractures, followed by low-angle fractures, accounting for 60.34% and 21.43% of the total number of observed fractures, respectively. Core observation shows that the core fracture length is 5-30 cm and the core fracture width is 0.1-0.6 mm.

The imaging images can identify fractures with different angles and filling degrees—Figure 1. The statistics of the Carboniferous imaging logging fractures in the Chepaizi area show that half-filled fractures and unfilled fractures account for 66% of the total number of identified fractures, with a high degree of effectiveness. High-angle fractures have the lowest filling degree, and low-angle fractures have the highest filling degree.

Taking well Che 482 in the Che 471 well area as an example, according to the characteristics reflected by the XRMI image data in Figure 2, the fracture types mainly include mesh fractures, oblique fractures, straight split fractures, induced fractures, filled-semifilled fractures, and microfractures. The Carboniferous fissures are related to the direction of faults and can be roughly divided into two groups, mainly near-EW-trending fissures (consistent with the average fault trend), followed by near-SN-trending fissures (consistent with the reverse fault trend).

2.2. Fracture Plugging Theory. Fracture leakage is one of the typically complex problems in the drilling process. There are currently two common solutions to plugging: active plugging and corrective plugging, depending on whether or not plugging occurs. In the process of actively strengthening the wellbore, the fracture tip is isolated from the wellbore pressure by the plugging material slurry, thereby preventing the expansion of the fracture. Corrective borehole strengthening is a method to effectively improve the fracture resistance of rock formations by improving the formation

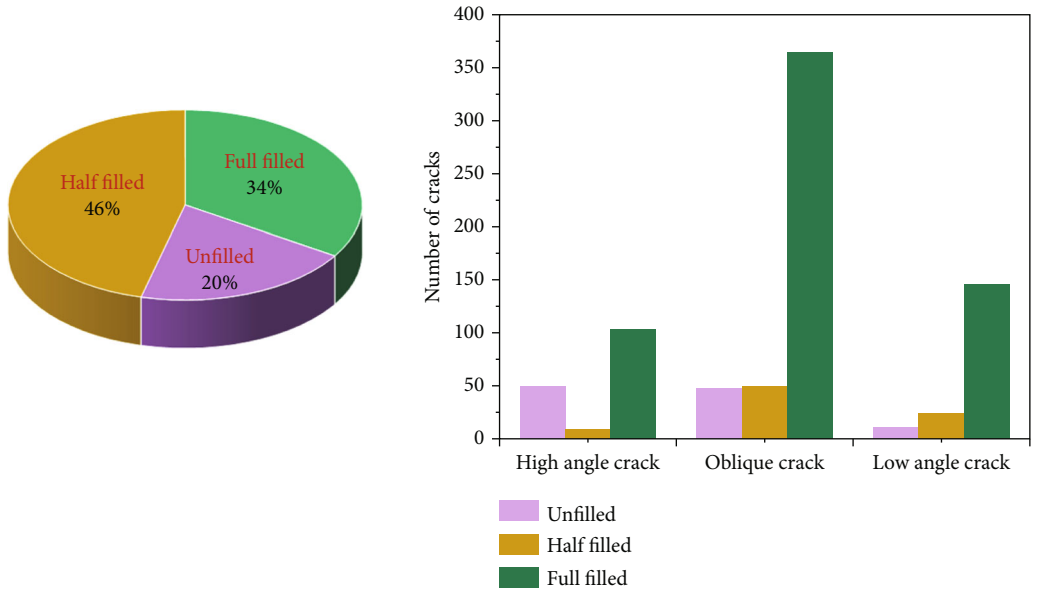

Figure 1: Characteristics of Carboniferous fractures in Chepaizi area.

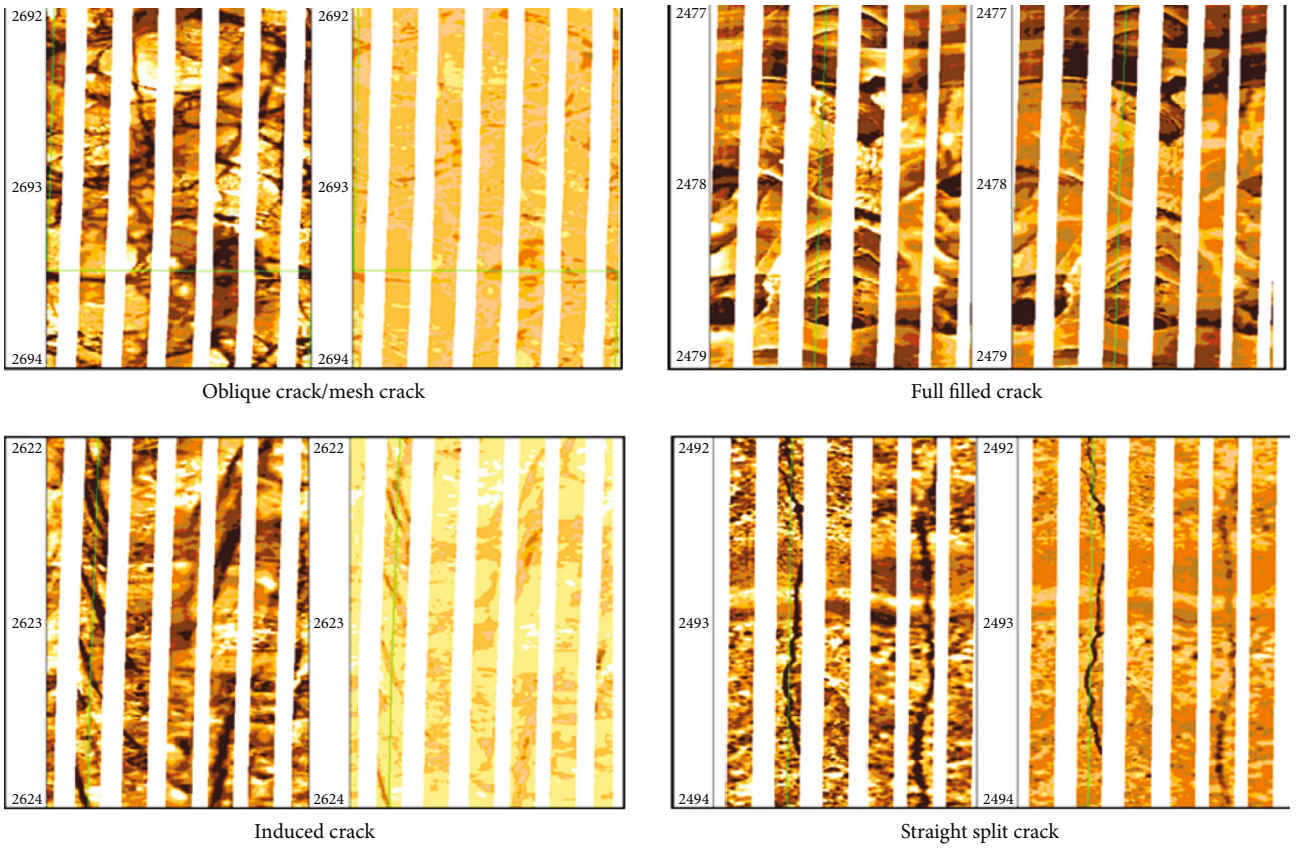

Figure 2: XRMI image characteristics of fractures in well Che 482.

closure stress and increasing the hoop stress in the near-wellbore area. The most common wellbore-strengthening theories are ring compression stress enhancement (stress cage) [28, 29], fracture propagation resistance (FPR) [30], and fracture closure stress (FCS) [31]. Figure 3 depicts the role of the plugging material in different wellbore-strengthening theories [32].

No matter which wellbore strengthening theory is adopted, it all involves the need to make the loss-stopping material be carried into the fracture so as to construct the

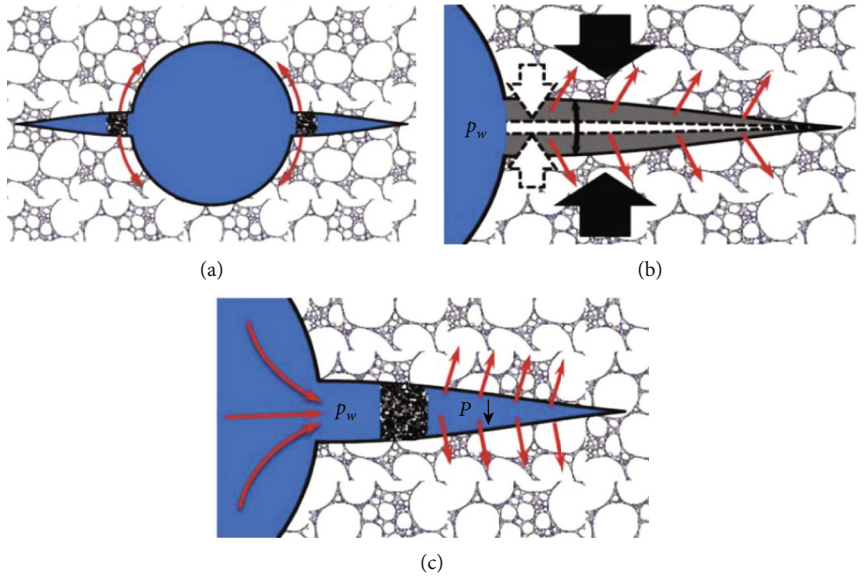

Figure 3: Common hypotheses related to mechanical wellbore strengthening. (a) Stress cage. (b) Fracture-closure stress. (c) Fracture-propagation resistance [32].

plugging zone. Loss-stopping materials are appropriately positioned within the fracture to isolate the pressure transfer in the fracture and increase the hoop stress in the near-wellbore region. This behavior is a complex process involving the migration behavior of particles in the fluid and the contact behavior between particles and particles and fractures.

The lost circulation material is carried into the fracture by drilling fluid or a particular lost circulation slurry. The behavior of fluid and particles in this transport process can be described by equations (1) and (2). According to the drilling fluid loss model in a single nonsite fracture established by Li et al. [33], for the non-Newtonian Heba drilling fluid, the flow velocity equation in the fracture is

$$V = \left(\frac{n}{2n+1}\right)\left(\frac{w}{2}\right)^{1+(1/n)}\left(\frac{1}{k}\right)^{1/n}\left(-\frac{d_p}{d_x} - \frac{2n+1}{n+1}\frac{2\tau_y}{w}\right)^{1/n}. \tag{1}$$

In the formula, n is the flow pattern index (dimensionless), K is the consistency coefficient (Pa▪s^n), τ_y is the dynamic shear force (Pa), P is the pressure (Pa) and w is the fracture width.

In the process of two-phase flow of the plugging material in the fluid, when the fluid in the fracture flows in a laminar flow state, the total drag force and drag force coefficients on the particles are equations (2) and (3), respectively:

$$F_d = C_D A_p \frac{\rho u^2}{2}, \tag{2}$$

$$C_D = \frac{24}{Re_p}, \tag{3}$$

where A_p is the surface area of the particle (cm^2), ρ is the density of the fluid, (g/cm^3), μ is the viscosity of the fluid (MPa▪s), and Re_p is the Reynolds number of the fluid.

Therefore, it can be found that the migration behavior of the plugging particles in the fluid is related to the density, size, and shape of the particles and the density, rheological properties, and velocity of the fluid. The particle size distribution of the plugging material has a significant impact on the fracture sealing efficiency. Whitfill [34] proposed that in fractures, the particle size distribution should be kept at about 50% of the fracture width, improving the bridging ability of the material between fractures. Alsaba et al. [35] also proposed a new standard; the D50 and D90 of the plugging material should be equal to or more excellent than 3/10 and 6/5 of the fracture width, respectively, which can effectively seal the fracture. In fact, different types of leakage-stopping materials have slightly different requirements for the particle size distribution of the leakage-stopping materials under the same fracture width. Therefore, before designing the particle size distribution of the leakage plugging material that is most suitable for fracture plugging, the type of leakage plugging material needs to be considered. This process needs to be determined through field plugging experience or some laboratory experiments.

2.3. Experimental Analysis of the Correlation Factors of the Missing Control Effect

2.3.1. Experimental Apparatus. Figure 4 is a schematic diagram of an experimental setup used to evaluate the plugging ability of the leakage plugging material to fractures. The device provides different pressures by pressurizing the fluid through a high-pressure nitrogen cylinder and can provide a maximum pressure of 10 MPa. The storage device of the plugging slurry contains a liquid level metering device that can measure the volume of the plugging slurry that is displaced into the fracture at each stage. The simulated fractures used were split using cores from the Carboniferous formation in the Chepaizi block. The advantage of this natural simulated fracture is that it can better simulate the roughness and bedding of the actual formation

fracture and the corresponding permeability. The length of the entire fracture is 20 cm. The front and rear ends of the clamping device containing simulated natural fractures are equipped with pressure sensors to record the pressure of the plugging slurry when it passes through the fracture. Once the leak-stopping material forms a good sealing layer in the fracture, the front-end pressure of the clamping device will rise rapidly. The pressure at this time represents the pressure that the sealing layer in the fracture can bear. The collection device of the plugging slurry can record the volume of the plugging slurry in the whole process. Finally, after the experiment is completed, the position of the plugging layer in the fracture can be measured by disassembling the natural simulated fracture device.

Based on the experience of on-site construction and laboratory experiments, we found that even if the plugging particles can form a suitable plugin for the fracture because the plugging position is close to the front end of the fracture or the fracture opening, it can withstand a high pressure. However, during the actual drilling process, due to the influence of downhole pressure fluctuations, the plugging layer at the fracture mouth fell off again, failing to plug. Therefore, to evaluate the effect of indoor leakage control more realistically, we evaluate the pressure-bearing capacity P (MPa) of the fracture sealing layer and measure the invasion depth L (cm) of the sealing layer in the fracture. These two aspects are used as the evaluation criteria for evaluating the sealing effect of the fracture.

2.3.2. Influence of Different Factors on the Effect of Plugging Experiments. The fracture size used in the fracture sealing experiment is a natural fracture with a size of 5 cm × 30 cm. The maximum applied pressure in the experiment is 8 MPa, and the carrier fluid used is the drilling fluid used in the field. The viscosity of the fluid is adjusted by adjusting the amount of the viscosifier. The displayed viscosity is the apparent viscosity of the drilling fluid. The original pumping pressure of the drilling fluid with the addition of lost circulation material was 1 MPa. The plugging material is the KZ-4 plugging particle, which is the most widely used KZ series plugging material in Chepaizi, with a particle size between 18 and 22 mm.

(1) Influence of the fluid properties of the carrier fluid on the leakage control effect

(2) Influence of pumping factors on leakage control effect

(3) Influence of plugging materials on the effect of leakage control

Through laboratory experiments, it is found that the effect of fracture loss control is not only related to the plugging material but also has a great relationship with the pumping pressure and fluid properties. Figure 5 shows that as the viscosity of the carrier fluid increases, the magnitude of the drag force exerted by the fluid on the particles increases. When the carried viscosity is greater than 30 MPa▪s, the plugging particles can be better carried to the fracture depth during the migration process, and the intrusion depth reaches 12 cm. The sedimentation velocity of the particles is also reduced, which avoids the increase in concentration caused by excessive accumulation and the formation of plugs at the fracture openings, which weakens the plugging quality. When the viscosity continues to increase, the penetration depth and pressure-bearing capacity no longer change. Figure 6 shows that with the increase of pumping pressure, although the pressure-bearing capacity can reach 8 MPa, the intrusion depth gradually decreases, from 12 cm to 1 cm. The reason is that when the particles and the particles and the wall are hindered, they cannot stay. The displacement speed of the particles also began to increase, and the particles could not enter into the fractures in a proper order, resulting in the chaos of the force chain between the particles and the fractures, and the fractures were blocked in advance. Figure 7 shows that when the concentration of particles is lower, at 10%, the particles cannot form a tight seal in the fracture. However, if the particle concentration is too high, it is not conducive to the displacement of the particles to the depth of the fracture.

Figure 8 shows the difference in the penetration depth of the formed plugging layer and the plugging state in different plugging experiments. Through experiments, it is found that the greater the invasion depth L (cm) of the plugging layer, the better the effect of the plugging layer and the greater the pressure it bears. However, during the experiment, when the pressure-bearing capacity reached the highest, there was a significant difference in the penetration depth. It shows that in the actual plugging process of on-site fractures, the leakage control effect of fractures has a significant relationship with the pumping parameters of construction, the properties, and concentrations of leakage plugging materials, and the properties of the fluid carried.

2.4. Determination of the Relevant Factors of the Leakage Control Effect of the Chepaizi Block. This study is to conduct machine learning on the leakage control effect of the Carboniferous fractured leakage formations in the Chepaizi block. The selection of data set types dramatically impacts the quality of machine learning. LCM particles are pumped into the reservoir section with the plugging slurry and enter the reservoir under the action of pressure difference. This process involves the interaction force between particles and fluids and between particles and fractures [36]. The suspending force and drag force generated by the fluid on the particles will obviously affect the suspension, bridging, and filling of the particles during the plugging process [37–38]. The particle size distribution and its own properties of LCM determine whether the "throat" of the fracture can be just plugged, so that the fracture channel can be converted into a porous channel [39]. Based on the results of laboratory experiments and the experience of on-site leakage accident handling, a large number of parameters on the site were screened, and three types of factors that had a strong correlation with the success rate of on-site leakage plugging were selected, namely, pumping parameters, type, and matching of plugging materials, the fluid properties of the carrier fluid.

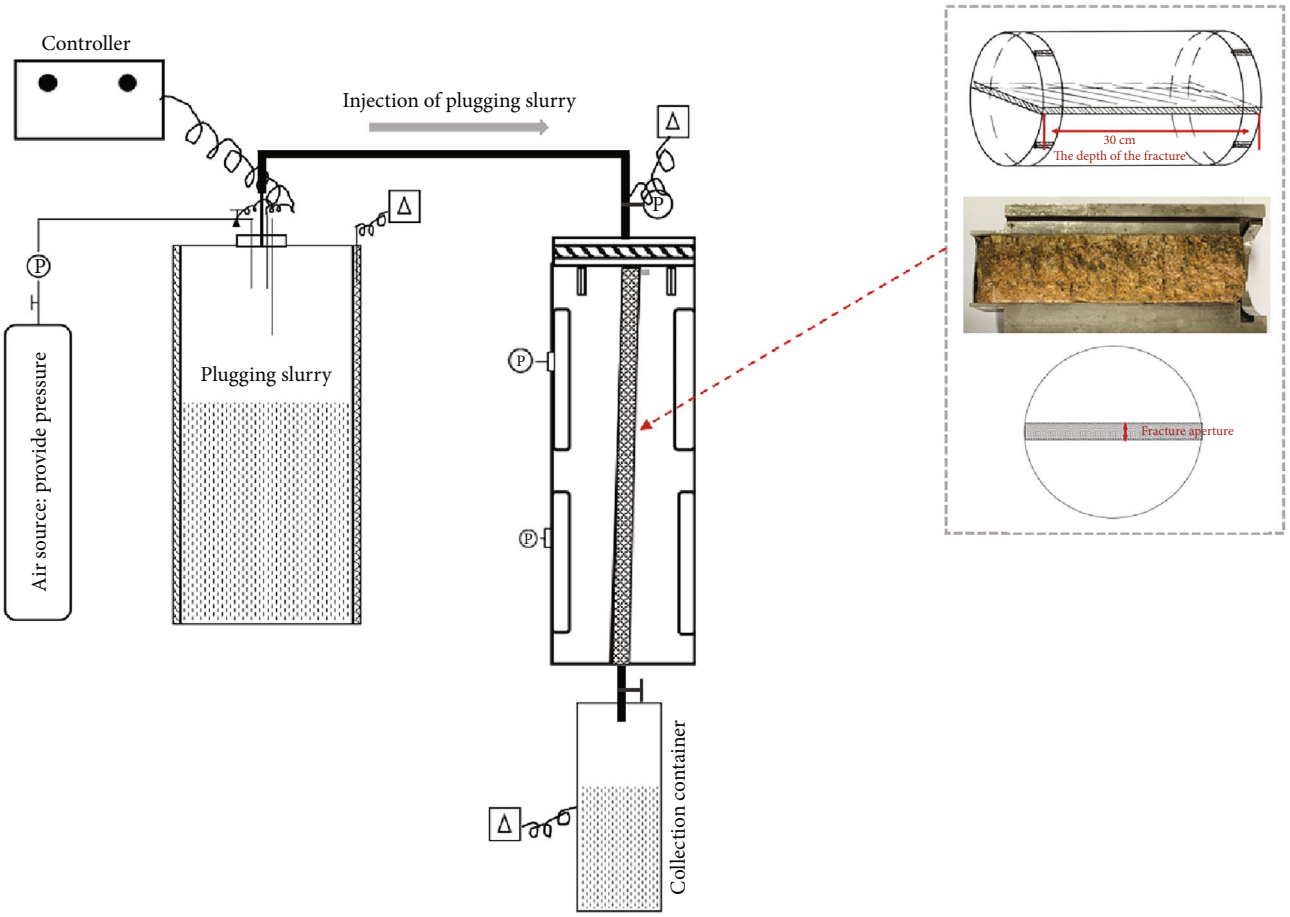

Figure 4: Indoor simulated natural fracture plugging an experimental device.

These three parameters can be further classified, and the same engineering factors can be divided into pumping displacement and maximum pumping pressure. The choice of the leakage-stopping material is the concentration of the leakage-stopping material and the type of the leakage-stopping material. The materials selected according to the type of on-site loss-stopping materials are KZ-3, KZ-4, KZ-5, walnut shell, vermiculite, comprehensive loss-stopping agent, and LWD-while-drilling agent. The fluid properties of the carrier fluid are divided into total volume, density, dynamic shear force, and funnel viscosity.

In the actual drilling process of the Carboniferous strata in the Chepaizi block, the leakage rate of each time has a certain difference. In fact, it is difficult to quantify the formation properties such as water swelling properties and heterogeneity. At the same time, we only study the leakage layer of the Carboniferous in this block, and other factors can be ignored, so the leakage velocity can be used as the description of missing stratigraphic characteristics. Finally, according to the parameters selected in the field, the field leakage control effect is defined. After each leakage plugging operation occurs, the actual leakage rate of the formation before and after the construction was compared. The leakage control effect is described in the form of a percentage, and the calculation formula is

$$E = 1 - \frac{V_{\text{initial}}}{V_{\text{after construction}}} \times 100\%. \tag{4}$$

In the formula, V_{initial} is the formation leakage rate before the plugging construction. The $V_{\text{after construction}}$ is the rate of formation leakage after on-site leakage plugging construction.

3. Artificial Neural Networks

When plugging the lost formation, the leakage control effect is affected by more than a dozen engineering parameters. When the information on the more than 400 times of plugging of more than 100 wells in the Carboniferous in this block is obtained after that, the neural network is applied to predict the leakage control effect of this block.

A neural network is a powerful tool for approximating unknown nonlinear functions [40], which helps solve different engineering problems and is now widely used in oil and gas exploration and development. The basic construction of a neural network is network construction, transfer function, and training method [41]. Neural networks build these

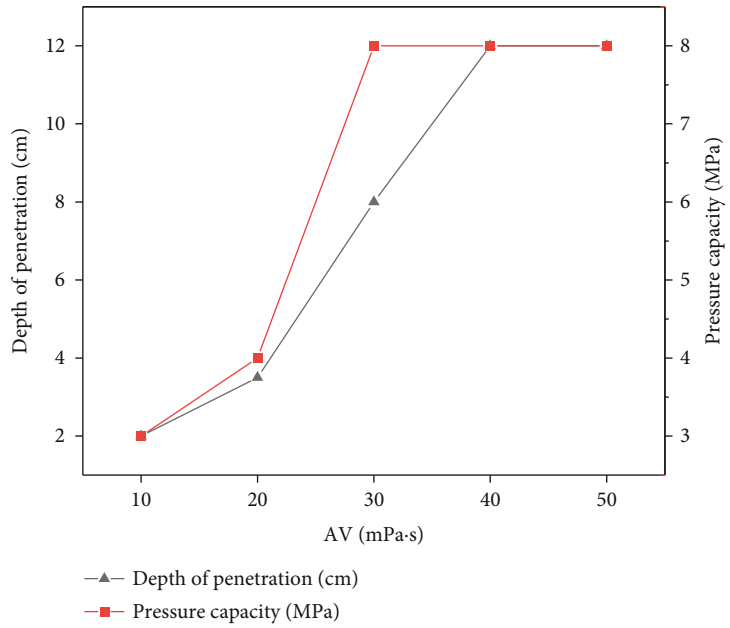

Figure 5: The effect of carrier fluid viscosity on the pressure-bearing capacity and invasion depth of the plugging layer.

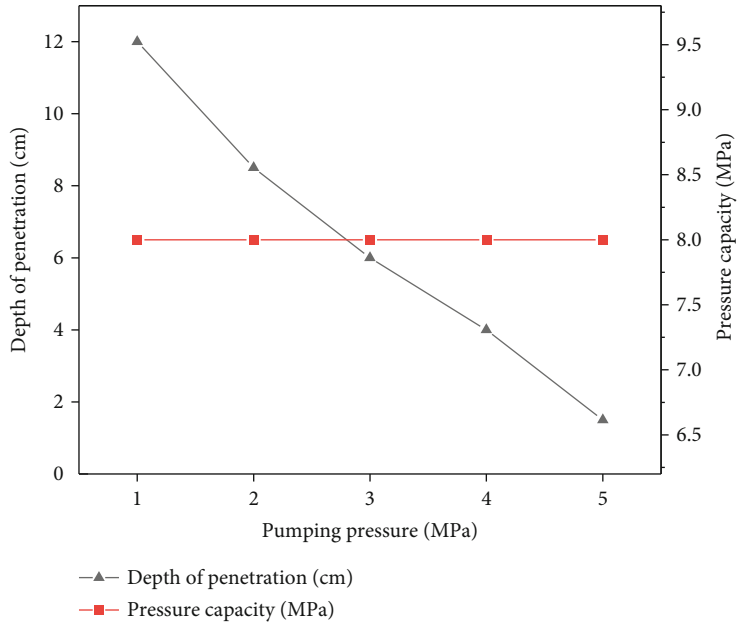

Figure 6: The effect of pumping pressure on the pressure-bearing capacity and invasion depth of the plugging layer.

network structures from neurons, including an input layer, an output layer, and one or more hidden layers. There is no connection between neurons in the same layer and forward connection between neurons in different layers [42]. The process of information propagation between neurons is divided into forwarding propagation and backpropagation. The output layer that does not get the expected value will say that the signal is transmitted back along with the originally connected node, and the desired goal is achieved by modifying the weight value.

We used logistic sigmoid and hyperbolic tangent transfer functions as activation functions. The logistic sigmoid and hyperbolic tangent transfer functions are considered to perform well for any problem involving fault diagnosis and feature classification. Logistic Sigmoid and hyperbolic tangent transfer functions are given by equations (5) and (6). Both functions are plotted in Figure 9. The model uses the Levenberg-Marquardt (LM) algorithm to find the extreme value of the function, which has the advantages of fast and efficient training and improving the convergence speed of

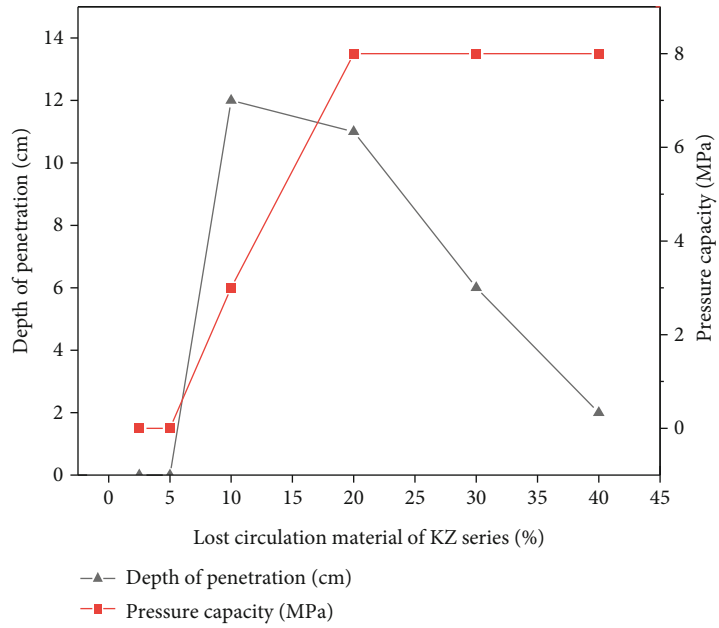

Figure 7: The effect of the concentration of the plugging material on the pressure-bearing capacity and invasion depth of the plugging layer.

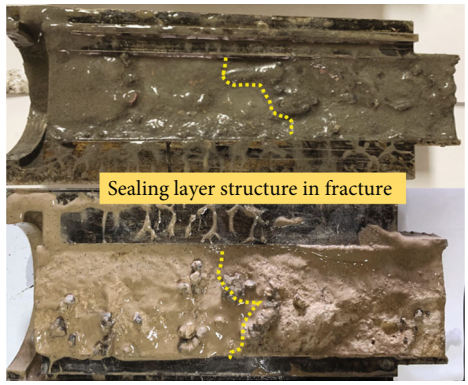

Figure 8: Experimental results of fracture plugging with different penetration depths.

ANN.

$$\text{Sigmoid} : \sigma(x) = \frac{1}{1 + e^{-x}}, \tag{5}$$

$$\text{Hyperbolic tangent} : \sigma(x) = \frac{e^{x} - e^{-x}}{e^{x} + e^{-x}}. \tag{6}$$

3.1. Data Collection and Preprocessing. Data sets play a crucial role in machine learning. A properly screened data set will improve the accuracy of predictions, while the introduction of redundant data sets will affect the prediction results. At the same time, the amount of data in the data set should be large enough to provide reliability for decision-making. In the 50 wells in the Chepaizi block, Xinjiang, China, fractured leakage occurred in different degrees in the Carboniferous strata, and each well had 3 to 5 fractured leakage behaviors, and each leakage plugging process took several times to block successfully. Therefore, according to the complex accident handling process in the drilling process recorded on the site, statistics and analyses are made about the on-site leakage plugging effect and various parameters in the actual construction process. Based on the empirical analysis of the on-site leakage plugging effect and the research on the relevant factors of the quality of the leakage plugging effect in the laboratory, this study selected the actual leakage rate on-site, the pump speed, and pump pressure during the construction process, and the matching and concentration of various types of leakage plugging materials. As well as the fluid properties (density, viscosity) of the carrier fluid as the data set used, these parameters are treated as independent variables. The leakage control effect is regarded as the dependent variable, and the leakage rate on-site will decrease to a certain extent after each leakage plugging construction. In order to digitize the leakage plugging effect on site, the actual leakage control effect is evaluated by taking the percentage reduction of the leakage rate before and after construction. When the on-site leakage plugging construction is completed, the leakage rate remains the same as before and does not decrease. At this time, the plugging quality is regarded as the worst, and 0% is used to represent the effect of this plugging construction. When the on-site leakage plugging construction is completed, the leakage rate decreases to 0, and the leakage plugging material smoothly enters the fracture to form a plugging layer to prevent the drilling fluid in the wellbore from leaking from the fracture again. At this time, the leakage control effect is the best, and the leakage rate decreases. The rate is 100%, and 100% is used to represent the effect of this plugging construction. In the 50 wells in the Chepaizi block, 450 cases (data sets) were collected.

In neural networks, high-valued data tends to increase the proportion of influence on the model, thus losing the features of low-valued data [43]. Therefore, it is necessary

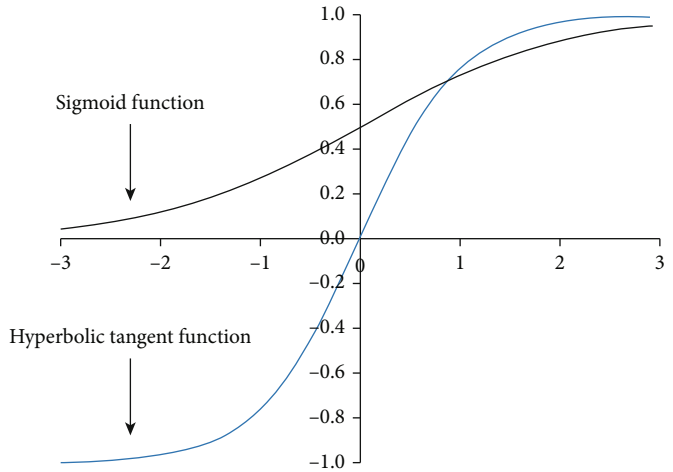

Figure 9: Schematic diagram of the hyperbolic tangent function and sigmoid function.

Table 1: Generated code for missing control-related parameters.

Column name	Overview	Code
Leak rate (m^3/h)	The rate of loss of drilling fluid during drilling	1
Displacement (m^3/h)	The rate at which the carrier fluid is pumped during the plugging process	2
Pumping pressure max (MPa)	The carrier fluid is pumped to the leakage layer, the pressure generated by the fluid at this time	3
Concentration (%)	The concentration of plugging particles in the overall plugging slurry	4
Addition of KZ-3 (t)	Plugging materials used in the field, mineral type granular plugging materials	5
Addition of KZ-4 (t)	Plugging materials used in the field, mineral type granular plugging materials	6
Addition of KZ-5 (t)	Plugging materials used in the field, mineral type granular plugging materials	7
Addition of walnut shell (t)	Plugging materials used on-site, plant-type granular plugging materials	8
Amount of vermiculite (t)	Leakage plugging materials used in the field, mineral type flaky leakage plugging materials	9
Amount of comprehensive plugging agent (t)	Composite leakage plugging material mixed with particles, flakes, and fibers	10
Addition amount of LWD agent (t)	Particle plugging material with particle size below 1 mm	11
Total addition (m^3)	The overall volume of carrier fluid	12
Density (g▪cm^3)	The density of carrier fluid	13
Funnel viscosity (s)	From the marsh funnel, indicating the viscosity of the drilling fluid	1 4
Actual blocking effect (%)	The ratio of the leakage velocity of the lost formation before and after the plugging construction	1 5

to normalize the data to avoid errors caused by the excessively large value range. Normalization of the data depends on the transfer function used to build the ANN.

When using logistic Sigmoid functions as the transfer function, with input and target data in the range (0, 1), use equation (7) to process the functions:

$$xn_i = \frac{(x_i - x_{\min})}{(x_{\max} - x_{\min})}. \tag{7}$$

Conversely, when using the TAANSIG transfer function, the input and target data are processed in the range (-1, 1) using

$$xn_i = \frac{2(x_i - x_{\min})}{(x_{\max} - x_{\min})} - 1. \tag{8}$$

Among them, xn_i represents the data set of plugging construction parameters after the standardization process is completed. x_i represents the original plugging construction parameter data set. $x_{\max}$ indicates the maximum value of the leakage plugging construction parameter data set, and $x_{\min}$ represents the minimum value of the leakage plugging construction parameter data set. Table 1 shows the generated codes for the relevant factors of the missing control effect.

Table 2: Statistical analysis and summary of sample data.

Types	Minimum	Maximum	Range	Arithmetic mean	Std. deviation	Skewness	Kurtosis
Leak rate (m^3/h)	3	100	9 7	51.37692	33.57244	0.430229	-1.35702
Displacement (m^3/h)	30	100.8	7 0.8	52.66154	18.32424	1.126849	1.879827
Pumping pressure max (MPa)	5	16	1 1	10.73077	2.739423	-0.02166	0.004141
Concentration (%)	0.05	0.3636	0.3136	0.109792	0.057074	3.442085	15.20886
Addition of KZ-3 (t)	0	2	2	0.461538	0.795698	1.350404	0.010491
Addition of KZ-4 (t)	0	2.5	2.5	0.942308	0.85852	0.238694	-1.44599
Addition of KZ-5 (t)	0	2.5	2.5	0.134615	0.510612	4.24259	18.6555
Addition of walnut shell (t)	0	3	3	1.923077	0.873678	-0.57641	-0.13565
Amount of vermiculite (t)	0	3	3	0.634615	0.915231	1.173339	0.043976
Amount of comprehensive plugging agent (t)	0	3	3	1.423077	1.080352	-0.17773	-1.36465
Addition amount of LWD agent (t)	0	2	2	0.134615	0.471448	3.500587	11.44695
Total addition (m^3)	11	80	69	55.42308	13.31042	-1.02063	3.95618
Density (g/cm^3)	1.15	1.25	0.1	1.221538	0.022819	-2.32647	5.916531
Funnel viscosity (s)	46	72	26	58.03846	9.500934	0.36903	-1.50663
Actual blocking effect (%)	0.1	1	0.9	0.596923	0.330102	0.280503	-1.75597

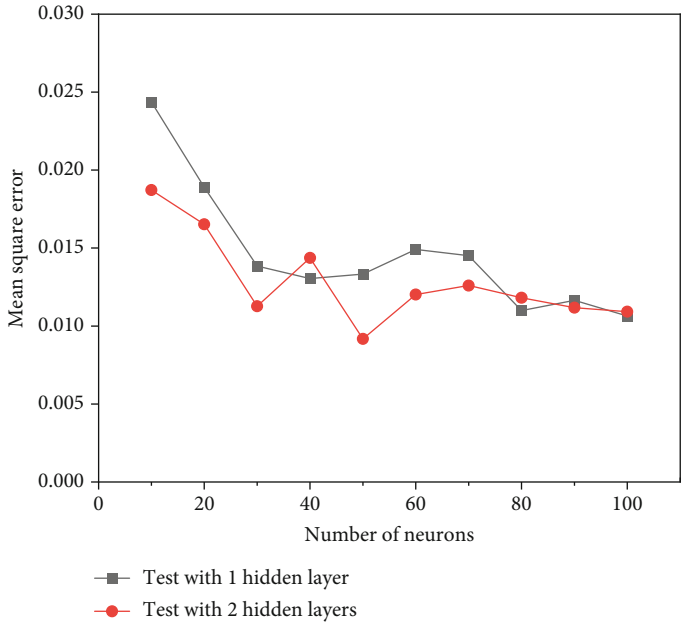

Figure 10: The MSE of an ANN model with different neurons and hidden layers (using the logistic Sigmoid functions).

Statistical analysis of the construction parameters and results of the plugging construction to determine the minimum value, maximum value, average value, range, standard deviation, skewness, and kurtosis of the data to be used. The data characteristics are shown in Table 2. We got a total of 4500 complete and valid data, including 22 data features.

3.2. Optimization and Evaluation of the Model. When using an artificial neural network, the statistical data set needs to be divided, and the standardized data set is randomly divided into a training data set and a test set. The training data set is used to tune the network weights and biases and compute gradients, and the test data set is used to test the developed model to evaluate its performance independently. The division ratio is related to the overall size of the data set. Based on the above, 80% of the data is used for training, and 20% is used for testing [44]. In the collected 450 sets of data sets, 360 sets of sample data are used for training, and 90 sets of sample data are used for testing. The training set and test set are suitable for the learning process, while the test set is used to test the ability of the model to achieve predictions.

This study used mean square error (MSE), mean absolute error (MAE), and coefficient of determination (R^2) as evaluation indicators. The formula is

$$\mathrm{MSE} = \frac{1}{n}\sum_{i}^{n}\left(P_{\mathrm{act}} - P_{\mathrm{pre}}\right)^2, \tag{9}$$

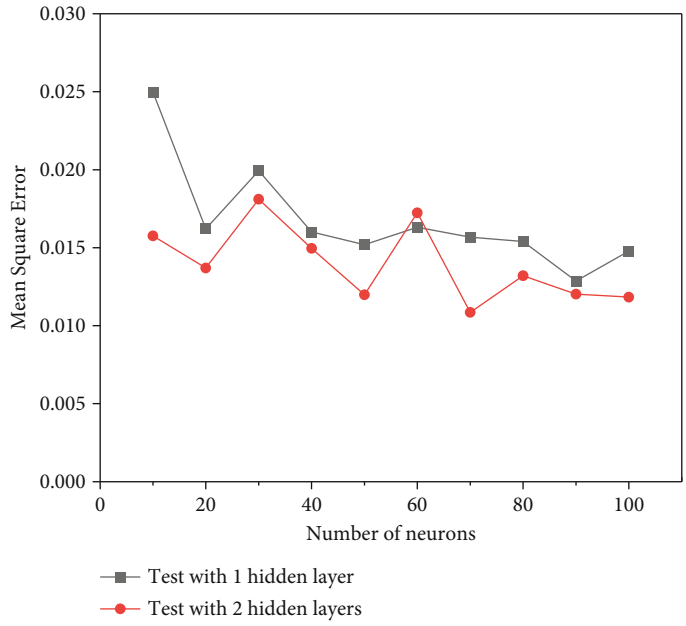

Figure 11: The MSE of an ANN model with different neurons and hidden layers (using the TASIG transfer function).

Table 3: Details of the developed artificial neural network architecture.

Feature	Value/model
Number of samples	450
Training algorithm	Levenberg-Marquardt algorithm
Hidden layer size	2L * 50N
Tolerance	1×10^{-6}
Maximum iteration	2000
Learning rate	0.07
Initial learning rate	0.01
Activation	Logistic sigmoid functions
Shuffle	TURE

$$\mathrm{MAE} = \frac{1}{m}\sum_{i=1}^{m}\left(P_{\mathrm{act}} - P_{\mathrm{pre}}\right), \tag{10}$$

$$R^2 = 1 - \frac{\sum_{i=1}^{n}\left(P_{\mathrm{act}} - P_{\mathrm{pre}}\right)^2}{\sum_{i=1}^{n}\left(P_{\mathrm{act}} - P_{\mathrm{ave}}\right)^2}. \tag{11}$$

In the above equation, y is the number of actually lost circulation solutions; $f(x)$ represents the number of correct simulated lost circulation solutions using machine learning methods; n is the total number of data types used for model evaluation. The proposed model has the highest sum R^2 and the lowest MSE, and MAE can be considered the best model.

4. Results and Discussion

4.1. The Architecture of ANN. The number of hidden layers, the number of neurons, and the transfer function are the key parameters that determine the accuracy of ANN, but there is no definite solution for the selection of ANN architecture. In order to find an ANN architecture suitable for this prediction model, it is necessary to conduct some experiments to determine the best configuration for ANN. Previous research has been done on the selection of the number of hidden layers and neurons, and some practical suggestions have been put forward. Boger and Guterman (1997) believed that hidden nodes should be at least as many as input nodes to capture 70%~90% of the features. Hecht-Nielsen proposed an empirical relationship between the number of computational hidden neurons and the number of input parameters, expressed in equation (11) [45]. Jiang et al. proposed a relational formula to determine the number of neurons in a multilayer hidden layer, and the relational formula is 12, where K, m_1, and m_2 are the number of neurons in the hidden layer, the number of input parameters, and the number of output parameters, respectively. m_3 is an empirical constant between 1 and 10 [46].

$$h = 2i + 1, \tag{12}$$

where h is the number of hidden neurons and i is the number of input parameters.

$$K = \sqrt{m_1 + m_2 + m_3}, \tag{13}$$

where K, m_1, and m_2 are the number of neurons in the hidden layer, the number of input parameters, and the number of output parameters, respectively. m_3 is an empirical constant between 1 and 10.

Based on the above features, we compare the prediction accuracy of each model by comparing the number of neurons in different hidden layers and the number of hidden layers. We control the number of neurons between 10 and 100. In order to control the complexity of the model and simplify the model, the number of hidden layers is set to 1

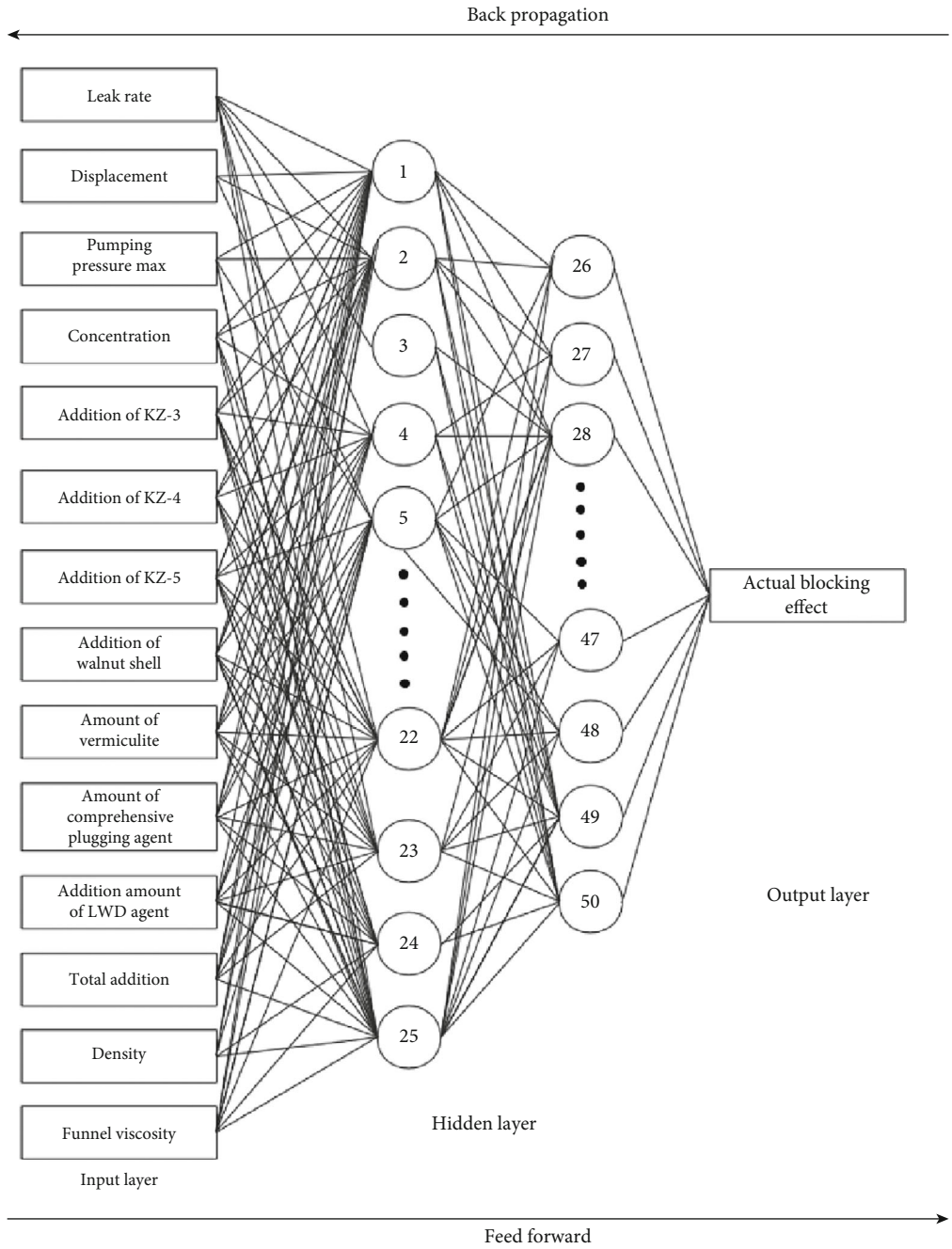

Figure 12: Topological structure of the ANN model established.

to 2 layers. Both TASIG and LOGSIG transfer functions were selected for testing. The prediction accuracy results obtained through different network structures are shown in Figures 10 and 11.

By changing the number of neurons in the hidden layer and the number of hidden layers, different transfer functions are used to analyze its impact on the performance of the model [47]. As shown in Figures 10 and 11, the ANN model's mean square error (MSE) varies with different model structures and is used to predict the effect of field leakage control.

With the increase in the number of neurons, the MSE of the ANN model shows a downward trend, and it can be found that the MSE of using two hidden layers is lower than that of using one hidden layer. When using logistic Sigmoid function s as the activation function of the hidden layer, as the number of neurons in the hidden layer continues to increase, the MSE gradually decreases, then increases, and then decreases again, until the number of neurons in the hidden layer reaches 80, and the MSE value of the model changes slightly. When the number of neurons is 50, the MSE is the lowest, which is 0.918%, and when using the TANSIG transfer function as the activation function, using two hidden layers, neurons with a quantity of 70 produced the best efficiency with an MSE of 1.08%. But an excessively high number of neurons have not been found to be more

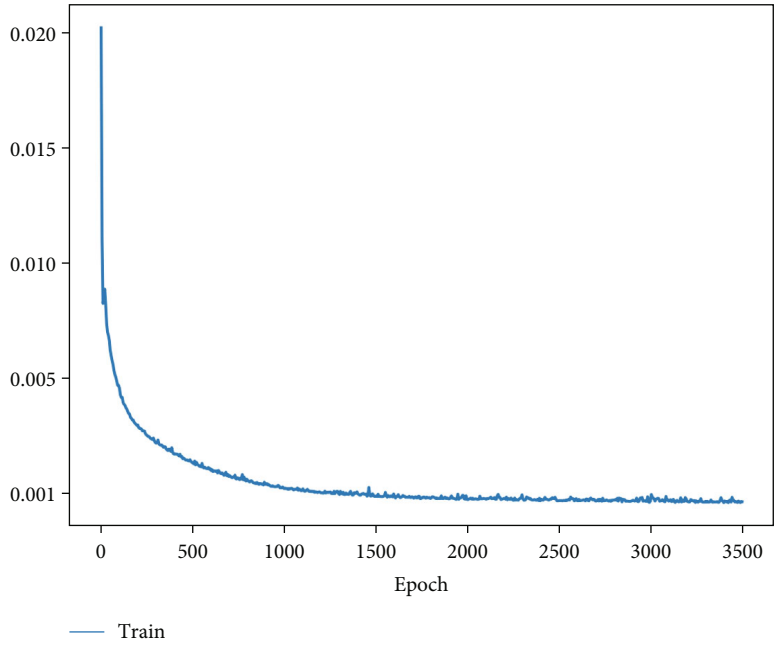

Figure 13: Variation of loss function during training and testing.

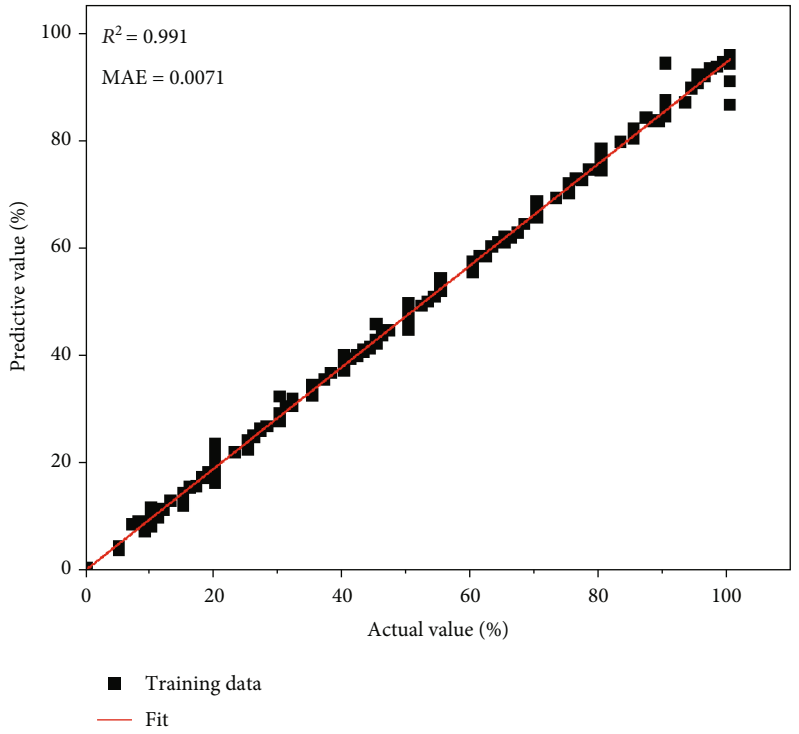

Figure 14: Model output and actual data: training data set.

efficient and can instead lead to higher error rates or longer convergence times, especially when training data is limited. The structure is simplified by comparing the prediction accuracy of the two structures and considering the reduction of the number of neurons as much as possible. The final selected ANN structure is shown in Table 3 and Figure 12.

4.2. Model Evaluation

4.2.1. Error Function. After determining the ANN model structure, input the data set. The mean square error (MSE) was chosen as the loss function. The error function decreases with increasing epochs during training and testing, as shown in Figure 13. After 2000 epochs, the loss function no longer

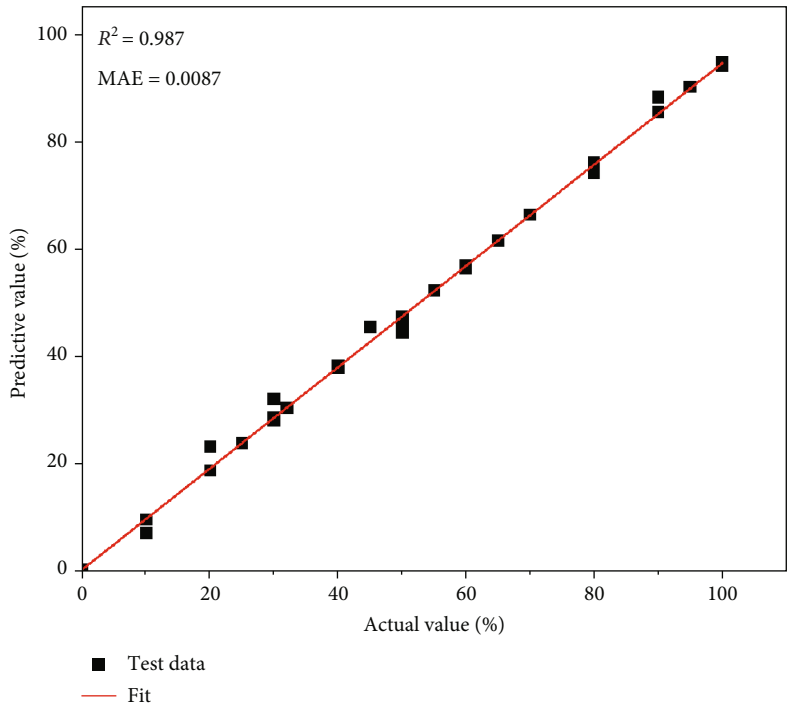

Figure 15: Model output and actual data: test data set.

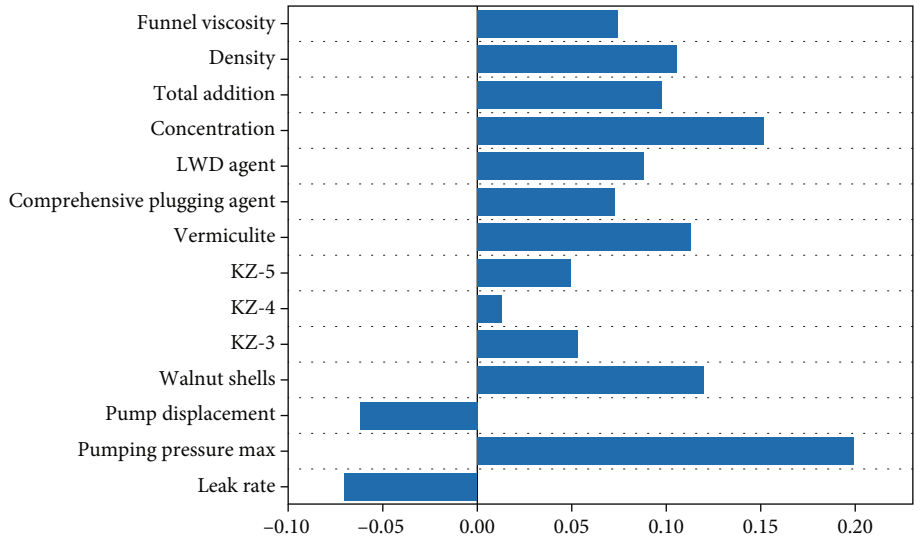

Figure 16: Correlation analysis between each characteristic data and the effect of missing control.

drops significantly and tends to stabilize. This means that the model does not need to increase the number of training times to improve its accuracy of the model.

4.2.2. Analysis of Accuracy. After selecting the best structure of the ANN, the accuracy of the model is characterized by the coefficient of determination R^2. Figures 14 and 15 show the difference between the predicted leaky control effect and the actual leaky control effect of the ANN model in the training and testing phases. The R^2 and MAE of the ANN model for the predicted target and the actual target for the training set were 0.991 and 0.0071, and the R^2 and MAE for the ANN model for the test data set using 20% of the data volume were 0.987 and 0.0087, which means that the model has high accuracy.

4.3. Correlation Analysis of Various Factors. The importance of individual features obtained from the model is shown in Figure 16. The figure shows the correlation of the maximum pumping pressure of the plugging slurry, the displacement, the formulation of the loss material, and the fluid properties of the carrier fluid on the actual loss control effect. The leakage size is considered to be negatively correlated with the leakage control effect. The more significant the leakage, the

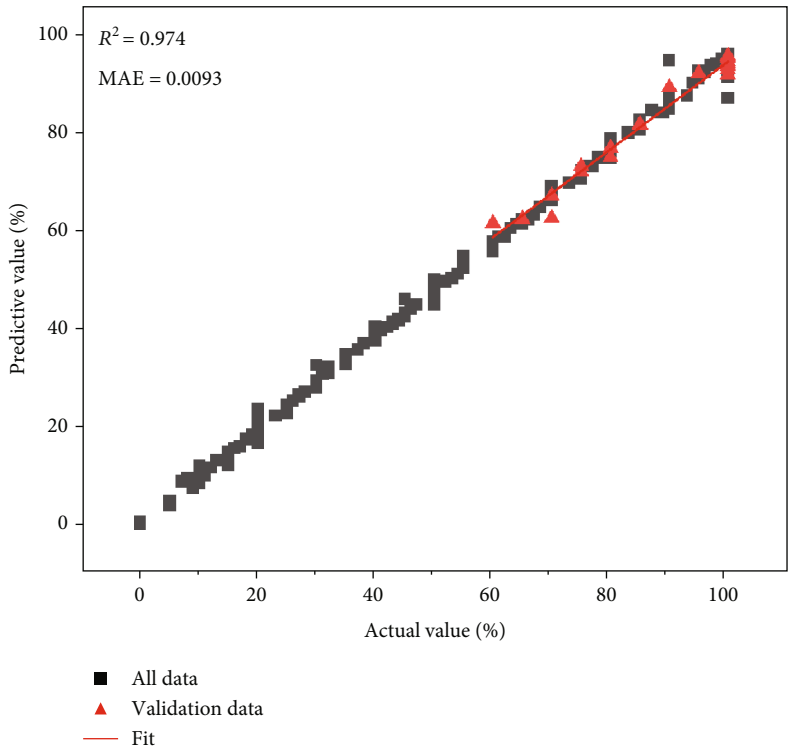

Figure 17: Validation of the model by the improved on-site leakage plugging case.

Table 4: Some real cases of fracture leakage plugging in Carboniferous strata in Chepaizi block.

Parameter	Well							
	A	B	C	D	E	F	G	I
Leak rate (m^3/h)	36	8	20	32.4	25	20	32.4	7.2
Displacement (m^3/h)	40.8	30	50.4	32.4	30	50.4	32.4	40.8
Pumping pressure max (MPa)	16	15	12	12	15	15	16	10
Concentration (%)	36	6	10	22.50	20	30	10	10
Addition of KZ-3 (t)	0	0	0	0	0	0	0	0
Addition of KZ-4 (t)	0	1.3	2	0	0	0	0	1
Addition of KZ-5 (t)	0	0	0	0	0	0	0	2
Addition of walnut shell (t)	2	0.5	3	3	2	3	2	0
Amount of vermiculite (t)	0	0	0	0	1	1	2	0
Amount of comprehensive plugging agent (t)	0	0	2	3	3	2	2	0
Addition amount of LWD agent (t)	2	0	0	3	0	3	0	0
Total addition (m^3)	11	30	60	40	30	30	60	30
Density (g▪cm^3)	1.21	1.1	1.22	1.14	1.21	1.22	1.13	1.14
Funnel viscosity (s)	50	49	52	48	52	53	53	45
Actual blocking effect (%)	100%	65%	100%	70%	90%	80%	95%	90%
ANN prediction (%)	9 9.81%	6 4.99%	9 7.63%	6 8.21%	9 2.08%	7 8.11%	9 6.12%	9 3.07%

worse the downhole plugging effect. In the plugging construction parameters, the size of the pumping displacement is negatively related to the plugging measures, and it is necessary to control the pumping displacement in the actual operation. The maximum pumping pressure has the strongest correlation with the leakage control effect, indicating that the maximum pumping pressure plays a great role in the leakage control effect. Among the leakage plugging materials, vermiculite and walnut shells have the most obvious effect. The irregular walnut shell has a higher friction coefficient with the fracture wall, which plays a better role in plugging in the fracture. The correlation strength of the concentration of the plugging material in the carrier fluid on the leakage control effect is second only to the maximum

pumping pressure. It shows that in the case of plugging construction implemented in Chepaizi block, the concentration of plugging materials needs to be further improved.

4.4. Data Verification of Actual Plugging Cases in the Field Using the ANN Model. Based on the analysis of the data by the model and the laboratory experiment research, further adjustments were made to the on-site leakage plugging formula system, and the corresponding construction parameters were adjusted at the same time. The plugging slurry is pumped into the lost formation with a displacement of 30~50 m^3/h in a low-displacement method, and the maximum pumping pressure is adjusted to more than 10 MPa to better squeeze the plugging slurry into the formation. At the same time, more flake materials vermiculite and walnut shells are used as plugging agents on site. At the same time, the concentration of the plugging material in the carrier fluid will further improve the leakage control effect of the field experiment.

Twelve times of plugging construction occurred in the following three wells. Use these 1 or 2 leak plugging construction data as a validation data set. Through the research on the actual leakage control effect in the field, as shown in Figure 17, it is found that the R^2 and MAE of the ANN model for the prediction target of the validation set and the actual target are 0.974 and 0.0093, indicating that the modified model has a good fit. Table 4 shows the detailed data of some cases after the improved plugging measures. After the adjustment of the plugging measures, the actual leakage control effect is greater than 65%, which has been dramatically improved compared with the previous one.

5. Conclusion

The prediction of the leakage control effect of the Carboniferous fractured leakage strata under the current leakage plugging construction measures in the Chepaizi block is studied by establishing the ANN model.

The experimental results show that the displacement pressure, the formulation of the plugging material, and the fluid properties of the carrier fluid play an important role in the leakage control effect of the fracture. In this study, through the analysis of on-site leakage plugging construction cases from a large number of construction parameters, a method for predicting the plugging effect of drilling site leakage plugging is proposed, and a set of ANN models with good accuracy is established.

The trained artificial neural network model can be well used to predict the performance of the plugging measures on the site of the subblocks of the car row. The trained model can produce predictions in seconds and is an excellent tool for evaluating the effectiveness of on-site leak plugging operations. In the subsequent 12 leakage accidents in three wells, the improved leakage plugging measures were applied, and the actual leakage control effect was obtained. Finally, the obtained data set is input into the model, which shows that the prediction results are in good agreement with the field application results, and the coefficient of determination $R^2 = 0.97408$.

This study provides a convenient and accurate way to effectively predict the effect of plugging measures in the Chepaizi block and provides help for the selection of reasonable construction parameters and optimal plugging slurry formulations. Due to different geological conditions and leakage reasons, the established model is only suitable for the Chepaizi subblock, and it still has certain limitations. In the future, we can try to collect more field data, and we can build a prediction model that can adapt to a wider range of blocks.

Data Availability

The [DATA TYPE] data used to support the findings of this study are available from the corresponding author upon request.

Conflicts of Interest

The authors declare that they have no conflicts of interest.

Authors' Contributions

Jianjian Song conceptualized the study and wrote, reviewed, and edited the manuscript. Lei Pu assisted the data curation, carried out formal analysis, and wrote the original draft. Lei Pu and Jun Zhou were responsible for methodology. Lei Pu and Shanshan Zhou contributed to the project administration. Jianjian Song and Jun Zhou were responsible for the resources. Jianjian Song and Mingbiao Xu supervised the study.

Acknowledgments

We would like to thank the Bakken Laboratory of Yangtze University for their support. At the same time, I would like to thank my friend Yuchen Zhang for her help. This research was supported by the Open Foundation of Cooperative Innovation Center of Unconventional Oil and Gas, Yangtze University (Ministry of Education and Hubei Province), No. UOGBX2022-02 and UOG2022-02.

References

[1] X. U. Chengyuan, J. Zhang, K. A. N. G. Yili et al., "Structural formation and evolution mechanisms of fracture plugging zone," *Petroleum Exploration and Development*, vol. 48, no. 1, pp. 232–242, 2021.

[2] L. Zhang, F. Zhou, W. Feng, M. Pournik, Z. Li, and X. Li, "Experimental study on plugging behavior of degradable fibers and particulates within acid-etched fracture," *Journal of Petroleum Science and Engineering*, vol. 185, article 106455, 2020.

[3] R. Li, G. Li, Y. Feng, X. Yang, Y. Teng, and Y. Hu, "Innovative experimental method for particle bridging behaviors in natural fractures," *Journal of Natural Gas Science and Engineering*, vol. 97, article 104379, 2022.

[4] Y. Feng, G. Li, and R. Li, "Influence of the lost circulation material injection method on the fracture plugging: a visualization experimental study," in *SPE/AAPG/SEG Unconventional Resources Technology Conference*, Austin, Texas, USA, July 2020.

[5] L. Zhang, Z. P. Li, F. P. Lai et al., "Integrated optimization design for horizontal well placement and fracturing in tight oil reservoirs," *Journal of Petroleum Science and Engineering*, vol. 178, pp. 82–96, 2019.

[6] L. Pu, P. Xu, M. Xu, J. Song, and M. He, "Lost circulation materials for deep and ultra-deep wells: a review," *Journal of Petroleum Science and Engineering*, vol. 214, article 110404, 2022.

[7] W. Sui, Y. Tian, Y. Zheng, and K. Dong, "Modeling temporary plugging agent transport in the wellbore and fracture with a coupled computational fluid dynamics–discrete element method approach," *Energy & Fuels*, vol. 35, no. 2, pp. 1422–1432, 2021.

[8] S. U. N. Jinsheng, B. A. I. Yingrui, R. Cheng et al., "Research progress and prospect of plugging technologies for fractured formation with severe lost circulation," *Petroleum Exploration and Development*, vol. 48, no. 3, pp. 732–743, 2021.

[9] G. Wang, C. Cao, X. Pu, and Z. Zhao, "Experimental investigation on plugging behavior of granular lost circulation materials in fractured thief zone," *Particulate Science and Technology*, vol. 34, no. 4, pp. 392–396, 2016.

[10] G. Wang, H. Du, and Z. Zhang, "Viscous behavior and wall slip of barite-weighted water-based drilling fluids containing a high particle fraction," *Journal of Petroleum Science and Engineering*, vol. 159, pp. 773–782, 2017.

[11] Y. Feng, G. Li, Y. Meng, and B. Guo, "A novel approach to investigating transport of lost circulation materials in rough fracture," *Energies*, vol. 11, no. 10, p. 2572, 2018.

[12] D. Feng, X. Li, X. Wang et al., "Water adsorption and its impact on the pore structure characteristics of shale clay," *Applied Clay Science*, vol. 155, pp. 126–138, 2018.

[13] X. Yan, Y. Kang, C. Xu, X. Shang, Z. You, and J. Zhang, "Fracture plugging zone for lost circulation control in fractured reservoirs: multiscale structure and structure characterization methods," *Powder Technology*, vol. 370, pp. 159–175, 2020.

[14] X. U. Chengyuan, Y. A. N. Xiaopeng, K. A. N. G. Yili, Y. O. U. Lijun, and J. Zhang, "Structural failure mechanism and strengthening method of fracture plugging zone for lost circulation control in deep naturally fractured reservoirs," *Petroleum Exploration and Development*, vol. 47, no. 2, pp. 430–440, 2020.

[15] J. I. A. Lichun, C. H. E. N. Mian, H. O. U. Bing, S. Zhen, and J. I. N. Yan, "Drilling fluid loss model and loss dynamic behavior in fractured formations," *Petroleum Exploration and Development*, vol. 41, no. 1, pp. 105–112, 2014.

[16] T. Zhang, F. Javadpour, Y. Yin, and X. Li, "Upscaling water flow in composite nanoporous shale matrix using lattice Boltzmann method," *Water Resources Research*, vol. 56, no. 4, article e2019WR026007, 2020.

[17] R. Albattat and H. Hoteit, "Modeling yield-power-law drilling fluid loss in fractured formation," *Journal of Petroleum Science and Engineering*, vol. 182, article 106273, 2019.

[18] M. B. Wang, Y. L. Guo, and W. Q. Chen, "Effect of solid particles on the lost circulation of drilling fluid: a numerical simulation," *Powder Technology*, vol. 363, pp. 408–418, 2020.

[19] H. Pang, H. Meng, H. Wang, Y. Fan, Z. Nie, and Y. Jin, "Lost circulation prediction based on machine learning," *Journal of Petroleum Science and Engineering*, vol. 208, article 109364, 2022.

[20] S. Gul and E. van Oort, "A machine learning approach to filtrate loss determination and test automation for drilling and completion fluids," *Journal of Petroleum Science and Engineering*, vol. 186, article 106727, 2020.

[21] M. B. Diaz, K. Y. Kim, H. S. Shin, and L. Zhuang, "Predicting rate of penetration during drilling of deep geothermal well in Korea using artificial neural networks and real-time data collection," *Journal of Natural Gas Science and Engineering*, vol. 67, pp. 225–232, 2019.

[22] A. A. Mahmoud, S. Elkatatny, and A. Al-AbdulJabbar, "Application of machine learning models for real-time prediction of the formation lithology and tops from the drilling parameters," *Journal of Petroleum Science and Engineering*, vol. 203, article 108574, 2021.

[23] Z. Zhu, X. Song, G. Li et al., "Prediction of the settling velocity of the rod-shaped proppant in vertical fracture using artificial neural network," *Journal of Petroleum Science and Engineering*, vol. 200, article 108158, 2021.

[24] I. Gomaa, S. Elkatatny, and A. Abdulraheem, "Real-time determination of rheological properties of high over-balanced drilling fluid used for drilling ultra-deep gas wells using artificial neural network," *Journal of Natural Gas Science and Engineering*, vol. 77, article 103224, 2020.

[25] G. Zhao, Y. Yao, L. Wang, C. D. Adenutsi, D. Feng, and W. Wu, "Optimization design of horizontal well fracture stage placement in shale gas reservoirs based on an efficient variable-fidelity surrogate model and intelligent algorithm," *Energy Reports*, vol. 8, pp. 3589–3599, 2022.

[26] L. Wang, Y. Yao, K. Wang, C. D. Adenutsi, G. Zhao, and F. Lai, "Data-driven multi-objective optimization design method for shale gas fracturing parameters," *Journal of Natural Gas Science and Engineering*, vol. 99, article 104420, 2022.

[27] A. K. Abbas, A. A. Bashikh, H. Abbas, and H. Q. Mohammed, "Intelligent decisions to stop or mitigate lost circulation based on machine learning," *Energy*, vol. 183, pp. 1104–1113, 2019.

[28] M. W. Alberty and M. R. McLean, "A physical model for stress cages," in *SPE annual technical conference and exhibition*, Houston, TX, USA, Sepetember 2004.

[29] R. Weijermars, "Stress cages and fracture cages in stress trajectory models of wellbores: implications for pressure management during drilling and hydraulic fracturing," *Journal of Natural Gas Science and Engineering*, vol. 36, pp. 986–1003, 2016.

[30] Z. Liu, M. Chen, and G. Zhang, "Analysis of the influence of a natural fracture network on hydraulic fracture propagation in carbonate formations," *Rock Mechanics and Rock Engineering*, vol. 47, no. 2, pp. 575–587, 2014.

[31] F. E. Dupriest, "Fracture closure stress (FCS) and lost returns practices," in *SPE/IADC Drilling Conference*, msterdam, The Netherlands, February 2005.

[32] C. Xu, Y. Kang, L. You, S. Li, and F. Chen, "High-strength, high-stability pill system to prevent lost circulation," *SPE Drilling & Completion*, vol. 29, no. 3, pp. 334–343, 2014.

[33] D. Li, S. Liu, Y. Kang, and Z. Hao, "Dynamic behavior of drilling fluid leakage in naturally# br# fractured formations," *Journal of Southwest Petroleum University (Science & Technology Edition)*, vol. 38, no. 3, p. 101, 2016.

[34] D. Whitfill, "Lost circulation material selection, particle size distribution and fracture modeling with fracture simulation software," in *IADC/SPE Asia Pacific Drilling Technology Conference and Exhibition*, Jakarta, Indonesia, August 2008.

[35] M. Alsaba, M. F. Al Dushaishi, R. Nygaard, O. M. Nes, and A. Saasen, "Updated criterion to select particle size distribution of lost circulation materials for an effective fracture sealing," *Journal of Petroleum Science and Engineering*, vol. 149, pp. 641–648, 2017.

[36] C. Lin, A. D. Taleghani, Y. Kang, and C. Xu, "A coupled CFD-DEM numerical simulation of formation and evolution of sealing zones," *Journal of Petroleum Science and Engineering*, vol. 208, article 109765, 2022.

[37] J. Zeng, H. Li, and D. Zhang, "Numerical simulation of proppant transport in hydraulic fracture with the upscaling CFD-DEM method," *Journal of Natural Gas Science and Engineering*, vol. 33, pp. 264–277, 2016.

[38] G. Wang, M. Dong, Z. Wang, T. Ren, and S. Xu, "Removing cuttings from inclined and horizontal wells: numerical analysis of the required drilling fluid rheology and flow rate," *Journal of Natural Gas Science and Engineering*, vol. 102, article 104544, 2022.

[39] G. Wang, Y. Huang, and S. Xu, "Laboratory investigation of the selection criteria for the particle size distribution of granular lost circulation materials in naturally fractured reservoirs," *Journal of Natural Gas Science and Engineering*, vol. 71, article 103000, 2019.

[40] V. D. Fachinotti, A. A. Anca, and A. Cardona, "Analytical solutions of the thermal field induced by moving double-ellipsoidal and double-elliptical heat sources in a semi-infinite body," *International Journal for Numerical Methods in Biomedical Engineering*, vol. 27, no. 4, pp. 595–607, 2011.

[41] D. A. Pandya, B. H. Dennis, and R. D. Russell, "A computational fluid dynamics based artificial neural network model to predict solid particle erosion," *Wear*, vol. 378, pp. 198–210, 2017.

[42] S. Smith, *Digital Signal Processing: A Practical Guide for Engineers and Scientists*, Elsevier, Amsterdam, Netherlands, 2013.

[43] M. T. Hagan, H. B. Demuth, and M. Beale, *Neural network design*, PWS Publishing Co, Boston, 1997.

[44] X. C. Zhang, J. G. Gong, and F. Z. Xuan, "A physics-informed neural network for creep-fatigue life prediction of components at elevated temperatures," *Engineering Fracture Mechanics*, vol. 258, article 108130, 2021.

[45] R. Hecht-Nielsen, "Theory of the backpropagation neural network," in *Neural Networks for Perception*, pp. 65–93, Academic Press, United States, 1992.

[46] Q. Jiang, R. Huang, Y. Huang et al., "Application of BP neural network based on genetic algorithm optimization in evaluation of power grid investment risk," *IEEE Access*, vol. 7, pp. 154827–154835, 2019.

[47] D. R. Baughman and Y. A. Liu, "Fundamental and practical aspects of neural computing," *Neural Networks in Bioprocessing and Chemical Engineering*, pp. 21–109, 1995.